Square patterns in rotating Rayleigh-Bénard convection

J. J. Sánchez-Álvarez,[1] E. Serre,[2] E. Crespo del Arco,[1] and F. H. Busse[3]
[1]*Departamento aFísica Fundamental, UNED, Apartado 60.141,28080 Madrid, Spain*
[2]*MSNM-GP UMR6181 CNRS/Universités d'Aix-Marseille I, II & III, La Jetée Technopôle de Château-Gombert, 38 rue Joliot-Curie, 13451 Marseille cedex 20, France*
[3]*Institute of Physics, University of Bayreuth, D-95440 Bayreuth, Germany*
(Received 12 November 2004; revised manuscript received 15 June 2005; published 27 September 2005)

The Küppers-Lortz instability occurs in rotating Rayleigh-Bénard convection and is a paradigmatic example of spatiotemporal chaos. Since the steady state of convection rolls is unstable to disturbance rolls oriented with an angle of about 60° with respect to the given rolls in the prograde direction [G. Küppers and D. Lortz, J. Fluid Mech. **35**, 609 (1969)], a spatiotemporally chaotic pattern is realized with patches of rolls continuously replaced by other patches in which the roll axis is switched by about 60°. Surprisingly and contrary to this established scenario, Bajaj *et al.* [Phys. Rev. Lett. **81** (1998)] observed experimentally square patterns in a cylindrical layer in the range of parameters where Küppers-Lortz instability was expected. In this paper we present square patterns which we have obtained in a numerical study by taking into account realistic boundary conditions. The Navier-Stokes and heat transport equations have been solved in the Oberbeck-Boussinesq approximation. The numerical method is pseudospectral and second order accurate in time. The rotation velocity of the square pattern increases linearly with the control parameter $\varepsilon = Ra/Ra_c - 1$, as in the experiment of Bajaj *et al.* Furthermore, it was observed that this velocity decreases when the aspect ratio of the cylinder increases. These results indicate that the square pattern appears when the flow is laterally confined. The range of ε for which this pattern is stable tends to vanish for more extended layers.

DOI: 10.1103/PhysRevE.72.036307 PACS number(s): 47.54.+r, 47.27.Te, 47.11.+j

I. INTRODUCTION

Convection in a fluid layer heated from below and rotating about a vertical axis has long been a favored subject in nonlinear fluid dynamics because of the onset of convection in the form of spatiotemporally chaotic motions. In contrast to the direct transition from a laminar to a turbulent state observed in shear flows, the chaotic state of a rotating convection layer is induced already at infinitesimal amplitudes of convection by the Küppers-Lortz (KL) instability [1]. Here it must be kept in mind that onset of convection in a rotating layer for Prandtl numbers of the order unity or larger is always supercritical (see Ref. [2]). Typically, convection rolls become unstable to disturbances in the form of rolls oriented with their horizontal axis at an angle of about 60° in the sense of rotation with respect to the original rolls. As the disturbance rolls grow and replace the original pattern they themselves become unstable to disturbance rolls with an angle of 120 ° relative to the orientation of the original rolls. As this process occurs in an uncorrelated fashion in patches throughout the convection layer, it involves a spatiotemporally chaotic state. Starting with the early experiment of Heikes and Busse [3], (see also Refs. [4,5]), the KL chaos has been investigated in numerous laboratory studies as in Refs. [5–8] as well as in numerical simulations as in Refs. [9–11]. Nevertheless, theory and experiment disagree with respect to the dependence on ε of typical length and time scales which describe the KL state. A possible explanation for these disagreements was suggested by Hu *et al.* [5] and is related to the sidewall, which generates defects traveling into the bulk (see also Ref. [12]). Since the defects travel at a constant speed rather than diffusively, they could influence the system interior. These authors conjectured that the defects break up the KL domain and thus alter the characteristic length and time scales.

In contrast to the nonrotating case, sidewalls exert a destabilizing effect in the case of a rotating layer. Experimental observations of the characteristics of traveling waves caused by the sidewall have been reported and investigated by many researchers (see, for instance, Zhong *et al.* [7], Hu *et al.* [5], Ning and Ecke [13], Liu and Ecke [14,15], and Ecke and Liu [16]). The convection waves attached to the wall propagate in the retrograde direction. For theoretical studies of the onset of convection caused by a sidewall we refer to Goldstein *et al.* [17], Herrmann and Busse [18], and Kuo and Cross [19]. The dynamics of the sidewall modes may be described by a complex Ginzburg-Landau (CGL) equation. The coefficients have been measured in experiments [13,14] and obtained from the solutions of the Navier-Stokes equations [20]. In Ref. [20] the mean flows originating from two counter-rotating traveling waves in an annular cavity have also been investigated.

Surprisingly, and contrary to theoretical predictions (Clever and Busse [21]), Bajaj *et al.* [22] observed in a $\Gamma = 4.8$ circular layer ($\Gamma = R/d$, with R the cavity radius and d the height of the layer) that for $\Omega \equiv 2\pi f d^2/\nu \geq 70$ (f is the rotation frequency and ν the kinematic viscosity) the nature of the pattern near onset changed. Instead of typical KL patterns, square patterns were found to be stable although the bifurcation remained supercritical. This pattern slowly rotates in the prograde direction relative to the rotating cylindrical box and qualitatively its properties are the same for argon at Prandtl number $\sigma = 0.69$ and for water at $\sigma = 5$. Thus, we are faced with a major disagreement with theoretical predictions in a parameter range where one might have expected the theory to be reliable.

It is possible to reproduce the square pattern in numerical simulations. A picture of a computed square pattern, obtained by solving numerically the Boussinesq equations with a forced circular confinement, is included in Fig. 43 of the review article of Bodenschatz, Pesch, and Ahlers [23]. However no quantitative results from these simulations have become available.

The purpose of this numerical study is to investigate the properties of the square pattern and its dependence on relevant parameters. Rotating Rayleigh-Bénard convection is examined in realistic cylindrical cavities of moderate aspect ratio ($\Gamma=3$ and 5) using a pseudo spectral technique. After describing the basic equations of the problem and the numerical methods employed for their solution in Sec. II, we discuss the main results obtained in Sec. III. In the choice of the parameters we are guided by experimental studies of Bajaj *et al.* [22] and Ecke and Liu [16]. In general, a good agreement between numerical simulations and experimental measurements is found. Additional results for which experimental counterparts do not yet exist will also be presented. Concluding remarks are given in Sec. IV.

II. MATHEMATICAL AND NUMERICAL MODELS

Rayleigh-Bénard convection is described by the Boussinesq equations for the velocity vector $\mathbf{v}$ and the heat equation for the temperature T relative to the rotating frame of reference as follows:

$$\frac{\partial \mathbf{v}}{\partial t} + v \cdot \boldsymbol{\nabla}\mathbf{v} = -\boldsymbol{\nabla}P - 2\Omega\hat{\mathbf{z}} \times \mathbf{v} + \boldsymbol{\nabla}^2\mathbf{v} + \frac{\mathrm{Ra}}{\sigma}T\hat{\mathbf{z}}, \quad (1)$$

$$\boldsymbol{\nabla} \cdot \mathbf{v} = 0, \quad (2)$$

$$\frac{\partial T}{\partial t} + \mathbf{v} \cdot \boldsymbol{\nabla}T = \frac{1}{\sigma}\boldsymbol{\nabla}^2 T, \quad (3)$$

where Ω is the Coriolis number defined in the introduction. The Prandtl number σ and the Rayleigh number Ra are defined by $\sigma=\nu/\kappa, \mathrm{Ra}=\alpha g \Delta T d^3/(\nu\kappa)$, where α, κ and ν are the thermal expansion coefficient, thermal diffusivity, and kinematic viscosity of the fluid; g is the gravitational acceleration and $\hat{\mathbf{z}}$ is the unit vector in the axial direction (opposite to the direction of gravity). $\Delta T = T_{\mathrm{hot}} - T_{\mathrm{cold}}$ is the temperature difference applied between the boundaries. The height $d, d^2/\nu$, and ν/d, are used as scales for length, time, velocity, respectively. The temperature is made dimensionless using $\Delta T: T=(T^*-T_r)/\Delta T$ where $T_r=(T_{\mathrm{hot}}+T_{\mathrm{cold}})/2$ and T^* is the dimensional temperature.

It is convenient to write these equations using a cylindrical polar coordinate system (r,θ,z). The corresponding velocity components are $\mathbf{v}=(u,v,w)$. The centrifugal force is not included because the limit of $(2\pi f)^2 R/g \ll 1$ is assumed.

Conducting as well as insulating boundary conditions for the temperature at the vertical sidewall have been considered. For the velocity, no-slip boundary conditions ($u=v=w=0$) apply on all walls since these are fixed in the rotating frame of the cavity.

The spatial discretization of the equations is achieved with a pseudo spectral collocation-Chebyshev expansion in both the radial and the axial directions and a Fourier-Galerkin method is used for the azimuthal dependence [24]. The velocity-pressure coupling problem has been overcome by the use of a projection scheme for time discretization [25], also called the fractional steps or splitting method, which consists in solving the momentum and the continuity

TABLE I. Summary of the numerical results. Ω_{sq} is the angular velocity rate of squares, Ω_w is the angular velocity rate of the wall mode, and ω_w is its angular frequency.

				Bulk						Wall	
Γ	Ω	σ	Ra_c	ε	$\Omega_{sq}(d^2/\nu)^{-1}$	$T_{osc}(d^2/\nu)$	k	$k=m/\Gamma$	m	$\omega_w(d^2/\nu)^{-1}$	$\Omega_w(d^2/\nu)^{-1}$
					Insulating sidewall						
5	274	6.4	33029	0.004	0.4×10^{-3}	58	8.4	5.2	26	−5.0	−0.192
				0.019	0.5×10^{-3}	23	8.5	5.2	26	−5.1	−0.196
				0.044		23	8.0	5.2	26	−5.2	−0.200
3	274	6.4	33302	0.016	0.2×10^{-2}	12	8.4	3.7	11	−5.087	−0.463
				0.032	0.5×10^{-2}	11	8.6	3.7	11	−5.134	−0.467
				0.057	0.8×10^{-2}	8	8.9	3.7	11	−5.207	−0.473
3	274	0.7	33302	0.016	-2.6×10^{-2}		7.5	3.7	11	−45.631	−4.148
				0.032			7.6	3.7	11	−45.873	−4.170
				0.057	-2.86×10^{-1}		8.3	3.7	11	−45.607	−4.237
3	180	0.7	19255	0.008			6.5	3.7	11	−32.911	−2.992
				0.023	-3.78×10^{-1}		7.1	3.7	11	−32.938	−2.994
				0.091			7.3	3.0	9	−34.773	−3.864
					Conducting sidewall						
5	274	6.4	33029	0.019	0.8×10^{-3}		8.6	7.8	39	−1.1	−0.029
3	180	0.7	19255	0.023			6.9	5.7	17	−12.004	−0.711
3	274	6.4	33302	0.016	2.4×10^{-3}	39	8.2	7.3	22	−5.68	−0.258

equations in two main steps. First, a predicted velocity field, which is not divergence-free, is computed from the discretized momentum equations. In a second step, this velocity field is corrected in order to satisfy the incompressibility constraint. Here, a preliminary step is introduced in which an intermediate pressure field is computed from the Navier-Stokes equations. This preliminary pressure, which is taken into account in the computation of the predicted velocity field, allows the normal pressure gradient at the boundary to vary with time. Moreover, it involves a better attainment of the incompressibility constraint at the boundary. The time scheme is semi-implicit and second-order accurate [26]. For $\Gamma=5$ spatial grids of $49\times128\times11$ and $49\times128\times19$ in the radial, azimuthal, and axial directions, respectively, have been employed, and grids with the meshes $35\times96\times9$ and $35\times96\times19$ have been employed for $\Gamma=3$. The time step used is $\delta t=7.3\times10^{-4}$. Numerical solutions were found to be nearly the same for both meshes except for small shifts in the critical value of the Rayleigh number. Details on the accuracy of the numerical method are given by Serre and Pulicani [26]. The performance of the solver has been optimized for a vector-parallel supercomputer, here a NEC SX5.

III. RESULTS

The numerical solutions have been obtained for $\sigma=6.4$ and 0.7. The nonlinear regimes have been studied numerically in cylindrical boxes with moderate aspect ratios of $\Gamma=3$ and 5, and for two rotation rates $\Omega=180$ and 274. A survey of the results is given in Table I.

The critical value of Ra is obtained by extrapolation of the Nusselt number $\mathrm{Nu}=\Phi/(K\Delta T/d)$ (Φ is the flux of heat and K is the coefficient of heat conduction), to its intersection with the conduction value Nu=1. We define a reduced control parameter $\varepsilon=\mathrm{Ra}/\mathrm{Ra}_c-1$. In both $\Gamma=3$ and 5 boxes the patterns encountered were qualitatively similar and cellular patterns have been found near the onset in a short range of ε, preceding a Küppers-Lortz-like state.

In typical experiments, shadowgraph visualization shows only the vertically averaged index-of-refraction variations. An analogous presentation of the numerical results can be obtained when the interesting properties of patterns are exhibited through suitable projections of the three-dimensional (3D) hydrodynamic description onto the 2D horizontal plane. In this paper, the results are shown by using a smoothed black and white representation of the isotherms in the horizontal plane at mid-height: dark regions indicate warm upflows and bright regions indicate cold downflows.

In the following we first discuss the results obtained for insulating sidewalls and $\sigma=6.4$, then turn to the conducting sidewalls with $\sigma=6.4$, and finally consider results obtained for $\sigma=0.7$.

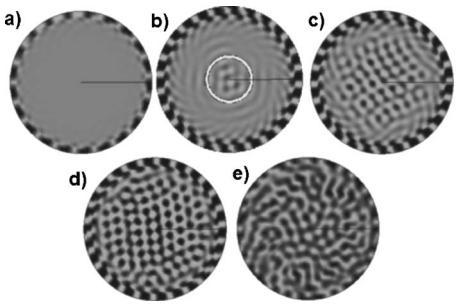

FIG. 1. Temperature pattern at mid-height for $\Gamma=5$, $\sigma=6.4$, $\Omega=274$ ($\mathrm{Ra}_c^{bulk}=33\,029$). Dark regions are warm upflows and bright regions are cold downflows. (a) Wall mode at Ra $=21\,380$, (b) rhombic pattern at $\varepsilon=0.0006$ (the white circle indicates the cellular pattern region), (c) square pattern at $\varepsilon=0.004$, (d) square pattern with a time dependence reminiscent of the Küppers-Lortz process at $\varepsilon=0.019$, and (e) spatially disordered pattern at $\varepsilon=0.22$.

A. Results for insulating sidewalls with $\sigma=6.4$

In the cylindrical box of $\Gamma=5$ with insulating sidewalls and rotating at $\Omega=274$, the flow patterns for $\sigma=6.4$ and for increasing values of Ra are shown in Fig. 1.

The conductive solution is stable at low Ra numbers ($\mathrm{Ra}\leqslant20\,000$) and the first transition to an oscillatory flow is due to the presence of the sidewall. It corresponds to the onset of a rotating wave which can be seen in Fig. 1(a) for $\mathrm{Ra}=21\,380$. There are 21 convective rolls traveling in the retrograde direction with an angular frequency of about $\omega_w=-3.8$ and a wave number $k=4.2$ [$(k=m/\Gamma)$, where m is the number of convective rolls around the circumference]. The sign of the frequency ω_w is defined by the dependence $\exp[i(m\theta-\omega_w t)]$ of the dominant Fourier component. As it is shown in Table II, the essential characteristics of this sidewall traveling wave are consistent with the experimental results [16,18] as well as with the results of the linear stability analysis [11,27]. The critical Rayleigh number for the convection in the bulk is $\mathrm{Ra}_c=33\,029$ ($\Omega=274$), which agrees well with Chandrasekhar's linear stability calculation [28] for a laterally infinite system ($\mathrm{Ra}_c=32\,840$ at $\Omega=270$). The shadowgraph of the flow at $\varepsilon=0.0006$ is presented in Fig. 1(b) and the convection pattern in the center does not show a clear regularity. Only at higher values of ε the pattern assumes fourfold coordination, it is seen in Figs. 1(c) and 1(d). The cellular pattern occurs within a circular region of radius

TABLE II. Characteristic parameters of sidewall convection. Results for insulating sidewall.

	Ra	σ	Γ	Ω	$\omega_w(d^2/\kappa)^{-1}$	$k(m/\Gamma)$
Ecke and Liu [16], experiments	21380	6.4	5	274	−3.5	
Ning and Ecke [13], experiments	21600	6.4	2.5	271	−3.6	4.39
Net and Mercader [27], linear stability analysis	22000	6.8	2.5	270	−3.5	3.6
Present results, direct numerical simulation	21380	6.4	5	274	−3.8	4.2

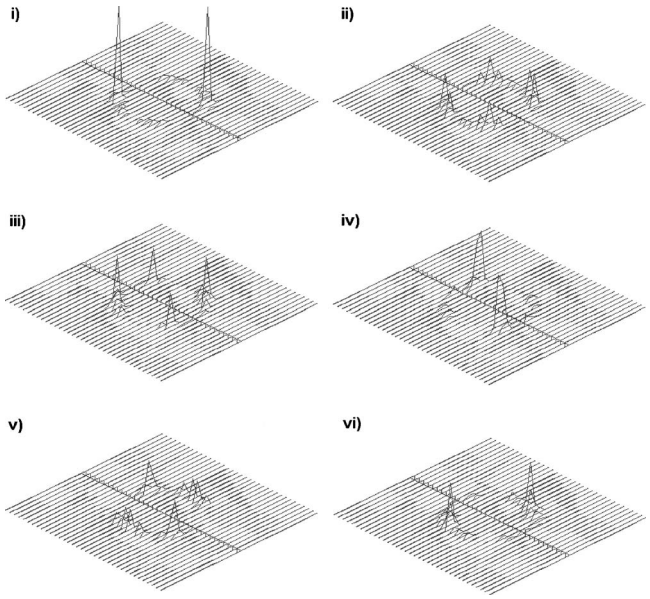

FIG. 2. A sequence of three-dimensional representations equidistant in time (from i to vi) with $\Delta t=60(d^2/\nu)$ showing the temporal evolution of the structure function. $\Gamma=5$, $\sigma=6.4$, $\Omega=274$, $\varepsilon=0.019$. The amplitudes of the two sets of rolls grow and decay in an alternating way.

R_{sq} that increases with ε [see Fig. 1(b) where $R_{sq}/\Gamma=0.3$ at $\varepsilon=0.0006$ and Fig. 1(c) where $R_{sq}/\Gamma=0.58$ at $\varepsilon=0.004$] to a maximum value $R_{sq}/\Gamma=0.75$, owing to the presence of the wall mode [Fig. 1(d)]. As the spiraling rolls emerging from the sidewall convection [Figs. 1(b) and 1(c)] indicate the interaction of the sidewall mode and the square pattern seems to occur over a fairly wide annular region.

Once the square cell pattern is established two types of time dependence can be distinguished. The amplitudes of the two sets of rolls with perpendicular axes of which the square cell pattern is composed grow and decay with time in an alternating way (see Figs. 2 and 3). A preferred direction is observed in the pattern when the amplitude of one set of rolls

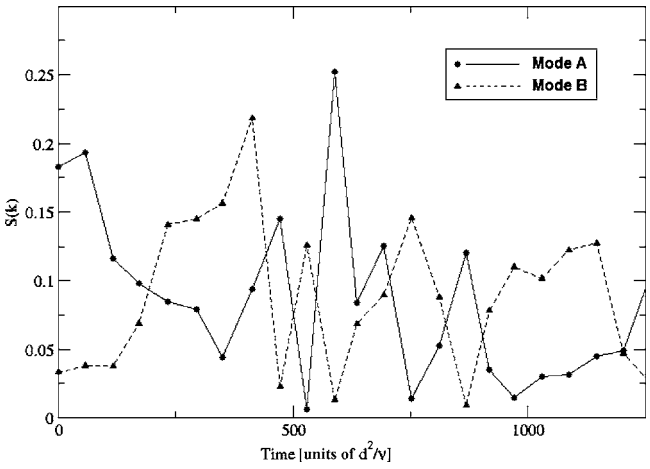

FIG. 3. Measurements of the square of the maximum amplitude of the two modes making up the square pattern at different time instants. ($\Gamma=5$, $\Omega=274$, $\sigma=6.4$, $\varepsilon=0.019$). The lines are only a guide to the eye.

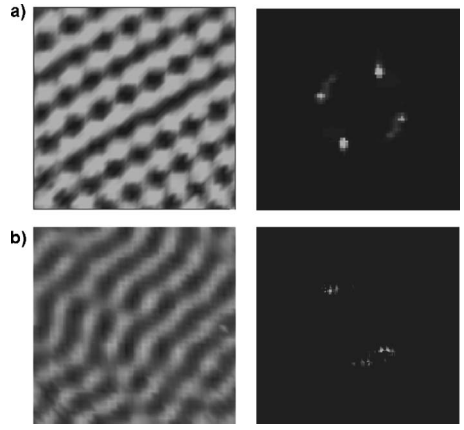

FIG. 4. On the left, patterns in the bulk are shown in the Cartesian frame centered on the axis of the cavity. On the right, corresponding structure function of the bulk region are plotted. The parameters are $\Gamma=5, \sigma=6.4$, $\Omega=274$, $\varepsilon=0.019$ (a) and (b) 0.044.

is more intense than that of the perpendicular set. The average period of this oscillation is indicated in Table I as T_{osc}. The second clearly distinguished time dependence is a slow rotation of the square pattern in the prograde direction. The corresponding angular velocity is indicated in Table I as Ω_{sq}

In order to characterize the spatial pattern we show the structure function $S(\mathbf{k})$ (square of the modulus of the Fourier transform) of the temperature at mid-height and for a region in the bulk [Fig. 4(a)]. At $\varepsilon=0.019$ the cells form a near-perfect square lattice, which slowly rotates in the direction of the system rotation (prograde direction) in agreement with experiments of Bajaj *et al.* [22].The angular velocity rate is $\Omega_{sq}\approx 5\times 10^{-4}$ (time is scaled with d^2/ν as in the definition of Ω) relative to the rotating frame of the cavity (Table I).

Results for $\Omega_{sq}(\varepsilon)$ are shown in Figs. 5(a) and 5(b) for both $\Gamma=5$ and 3 cavities, respectively. In Fig. 5(a), a numerically derived point at $\varepsilon=0.019$ is represented together with experimental results of Bajaj *et al.* [22] obtained at larger ε and for $\Omega=170, \sigma=5.4$, and $\Gamma=4.8$.

The results show that Ω_{sq} depends linearly on ε and that $\Omega_{sq}(\varepsilon)\to 0$ when $\varepsilon\to 0$, as suggested by the experimental results [22].

The flow is thus composed of two patterns: a square pattern slowly rotating in the bulk together with azimuthally periodic rolls adjacent to the circular sidewall (wall convection mode). As previously mentioned, the wall mode is traveling much faster in the opposite direction with a frequency $\omega_w\approx -5$ which is nearly independent of ε. The wall mode is associated with a mean zonal flow the average of which over time and over the z coordinate has been plotted in Fig. 6. This zonal flow is too weak to explain the rotation of the square pattern. It also has the wrong direction and is confined to the region of the sidewall convection.

The square pattern is stable in a narrower range of ε ($\varepsilon<\varepsilon_{max}=0.019$ at $=274$) than in experiments [22] performed at slower rotation rates: $0\leqslant\varepsilon\leqslant\varepsilon_{max}=0.13$ at $\Omega=170$ and $0\leqslant\varepsilon\leqslant\varepsilon_{max}=0.12$ ($\Omega=181$). This behavior suggests that at still higher Ω square patterns may disappear.

At larger $\varepsilon, \varepsilon>\varepsilon_{max}$, the flow exhibits some elongated parallel rolls which rotate and undergo sudden changes of

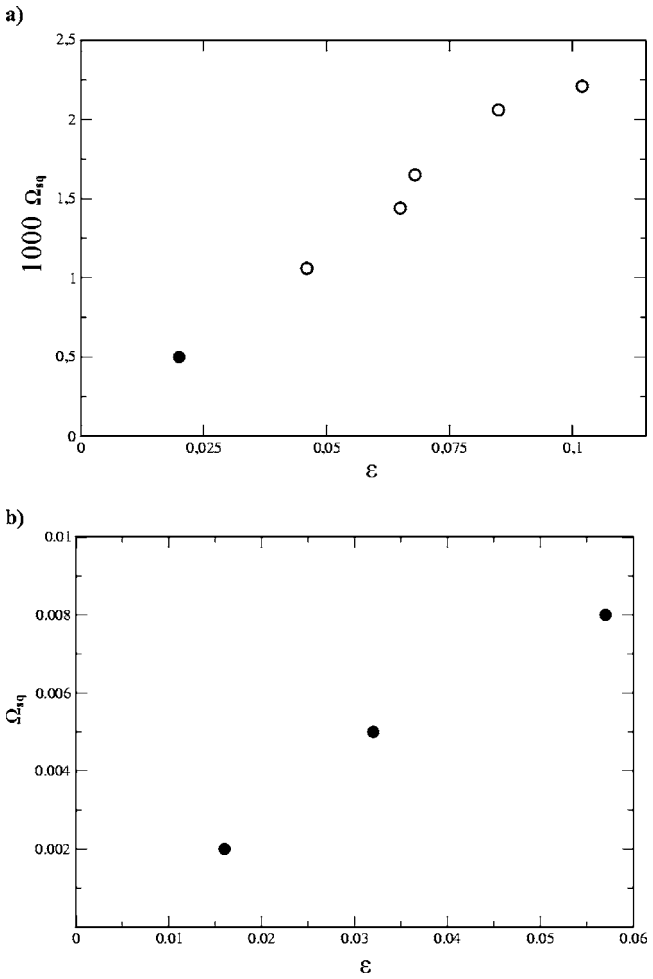

FIG. 5. (a) The rotation rate Ω_{sq} of the square lattice for $\Omega=274$, $\Gamma=5$, and $\sigma=6.4$ (solid point) and the results of Bajaj *et al.* [22] for $\Omega=170$, $\Gamma=4.8$, and $\sigma=5.4$ (empty points). (b) The rotation rate Ω_{sq} of the square lattice for $\Omega=274$, $\Gamma=3$, and $\sigma=6.4$. Time is scaled with d^2/ν.

preferred direction as expected on the basic of the KL instability. The switching angle is about 50° in the present case (see for example Fig. 7). The corresponding structure function $S(\mathbf{k})$ is shown in Fig. 4(b). At $\varepsilon=0.22$ the pattern seems more spatially disordered [Fig. 1(e)], with shorter rolls wandering, breaking, and forming preferred orientations that change in discrete steps. Visualizations at different time steps reveal that the orientation changes are discontinuous. The average wave number of this state is $k=8.2$.

In the smaller-aspect-ratio cavity, $\Gamma=3$ (insulating sidewall), convection in the bulk sets in at a slightly higher Rayleigh number ($\mathrm{Ra}_c=33\,302$) for $\sigma=6.4$ at $\Omega=274$ than in the $\Gamma=5$ cavity ($\mathrm{Ra}_c=33\,029$). At $\varepsilon=0.032$ the time behavior is oscillatory near the sidewall, associated with a wall mode that rotates with retrograde angular velocity $\Omega_w=-0.467(\Omega_w=\omega_w/m)$, and in the bulk, the square pattern rotates with $\Omega_{sq}\approx 0.005$. The rotation rate of the square pattern is much faster (by about ten times) than in the $\Gamma=5$ cavity (Fig. 5) suggesting that Ω_{sq} strongly decreases with increasing Γ. This result confirms the expectation of Ref. [22] and indicates again that the rotation of the squares is a property

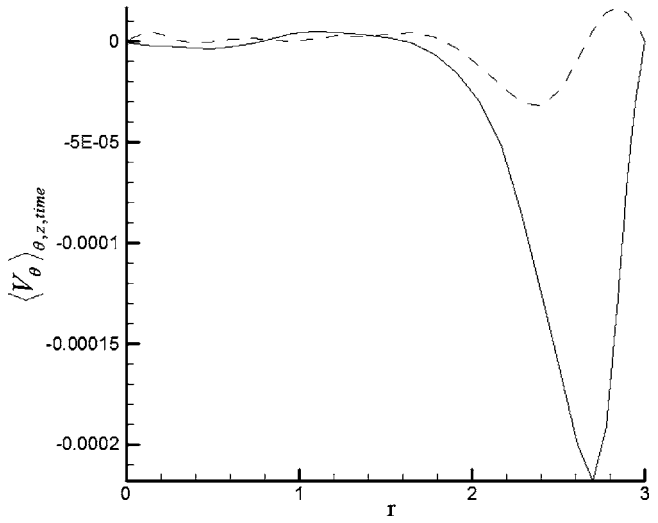

FIG. 6. Azimuthal mean flow averaged over vertical direction and time for $\Gamma=3$, $\Omega=274$, $\sigma=6.4$, $\varepsilon=0.016$, conducting (dashed line) and insulating (solid line).

of the finite system. As mentioned above, at larger $\varepsilon(\varepsilon=0.057)$, the pattern and its dynamics exhibit similarities with the Küppers-Lortz instability.

B. Results for conducting sidewalls with $\sigma=6.4$

Since the critical Rayleigh number for onset of sidewall convection increases with the thermal conductivity of the sidewall (see, for example, Ref. [18]) sidewall convection is much weaker in the case of a well-conducting sidewall. The intensity of the sidewall convection decreases by about 85% and 80% for $\Gamma=5$ and 3, respectively, when the thermal conductivity is increased from zero to higher values at a Rayleigh number of the order of 33 500. Consequently the mean flow generate by the sidewall convection in the conducting case is also weaker as indicated in Fig. 6. The mean zonal flow in the interior is essentially negligible.

The wave speed of sidewall convection is lower (Table I) and the bulk pattern extends closer to the wall than in cases with insulating boundary conditions [see Figs. 8 and 1(d)]. For this reason a very regular square pattern can be formed even in the case $\Gamma=3$ as shown in Fig. 9. In the case of insulating sidewalls the dominance of the sidewall convection usually prevents the establishment of such a regular pattern. While the regular square pattern in Fig. 9 lasts for about 110 vertical diffusion time, it is subsequently followed by an

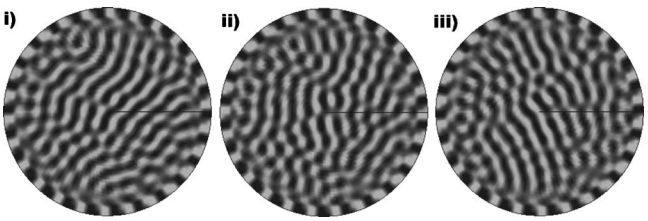

FIG. 7. KL state for $\Gamma=5$, $\sigma=6.4$, $\Omega=274$ at $\varepsilon=0.044$. The pattern is shown at three subsequent time steps separated by the time $2.92(d^2/\nu)$.

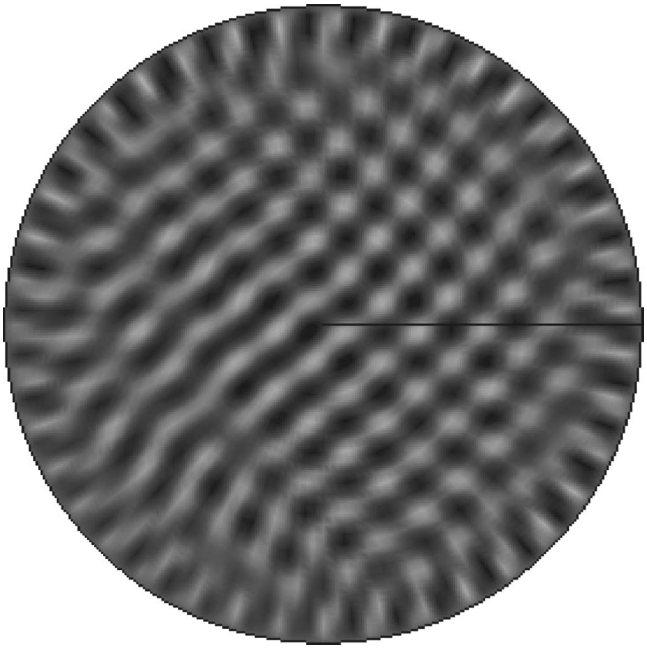

FIG. 8. Square pattern with a conducting sidewall for $\Gamma=5$, $\sigma=6.4$, $\Omega=274$ at $\varepsilon=0.019$. The initial condition is the one obtained at the same Rayleigh number using an insulating sidewall [Fig. 1(d)].

interval of more irregular pattern. Only after another interval of 100 diffusion time it tends to return to a regular square pattern. This intermittent dissolution of the square pattern and its reappearance reminds one of the similar process seen in the experiment of Bajaj *et al.* [22]. Less clearly seen in the experiments is the oscillation of the roll components. Even in the regular phase of the square pattern the two roll components of the square lattice vary in their amplitude as shown in Fig. 10.

C. Results for $\sigma=0.7$ in the case of insulating sidewalls

Simulations in the $\Gamma=3$ cavity have also been performed at a smaller Prandtl number, $\sigma=0.7$. The critical Rayleigh numbers and wave numbers do not change much with the Prandtl number (Table I) as expected from linear theory [28]. Nevertheless, the wall mode extends further into the bulk and forms spiral arms still rotating in the retrograde direction, but with about nine times larger velocity than at $\sigma=6.4$ (Table I). In the interior, the pattern is still cellular, but the flow tends to organize a hexagonal structure with sixfold symmetry [Fig. 11(a)]. The pattern is dynamically disrupted by many defects originating in the transition region between the bulk pattern and the wall mode structure. The interaction between both structures appears to be stronger than at $\sigma=6.4$. Further, the influence of the wall structures is so large at $\sigma=0.7$ that the bulk mode is now swept by the wall mode. The near 2:1resonance of the $m=11$ wall mode and the $m=6$ bulk pattern is sufficient to drive the bulk pattern in the retrograde direction, at least in the time average. At the lower value $\Omega=180$ the coupling between sidewall and outer bulk pattern is even stronger than at $\Omega=274$ because of the near

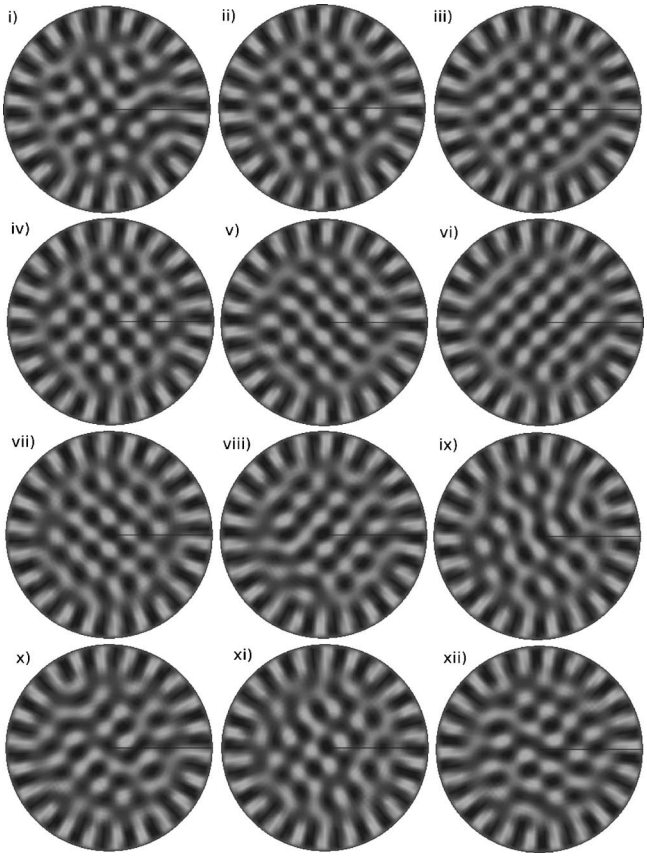

FIG. 9. Temporal evolution of the pattern for $\Gamma=3$, $\Omega=274$, $\sigma=6.4$, $\varepsilon=0.016$ with conducting sidewalls. The time between two figures (from i to xii) is $\Delta T=21.9(d^2/\nu)$.

1:1 resonance with the $m=9$ wall mode. The bulk pattern actually separates into three concentric-ring-like structures which rotate with increasing rate with increasing radius as indicated in Fig. 11(b). Certain jumps in the angular orientation seem to occur.

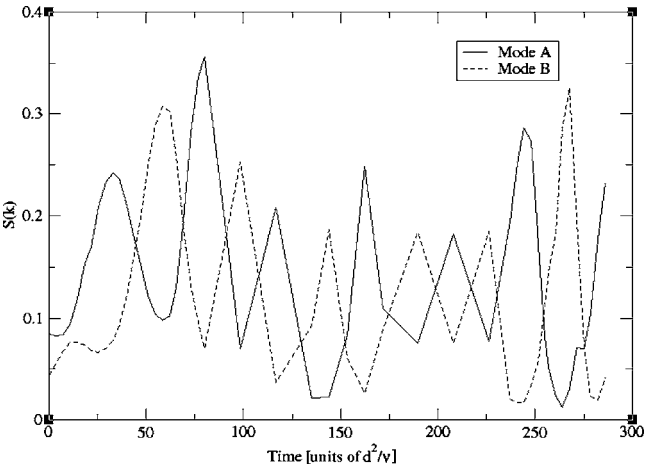

FIG. 10. Temporal evolution of the square of the maximum amplitude of the two modes making up the square pattern. $\Gamma=3$, $\Omega=274$, $\sigma=6.4$, $\varepsilon=0.016$, conducting sidewalls.

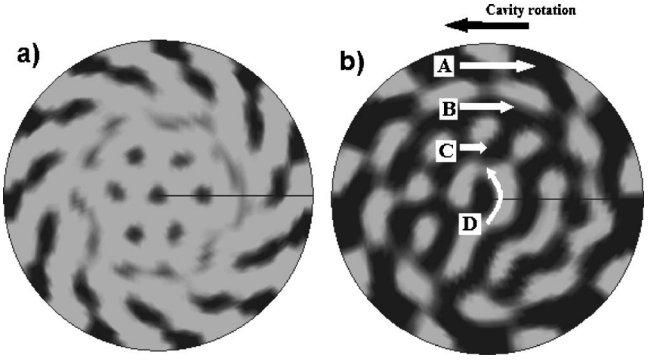

FIG. 11. (a) Cellular patterns for $\sigma=0.7$, $\Gamma=3$, $\Omega=274$ close to the onset of bulk convection ($\varepsilon=0.016$), showing hexagonal structures in the bulk and spiral arms related to wall convection. (b) Disordered cellular patterns for $\sigma=0.7$, $\Gamma=3$, $\Omega=180$, and $\varepsilon=0.091$. The bulk pattern separates into three concentric-ring-like structures which rotate with different velocities, $\Omega_A=-3.9$, $\Omega_B=-1.6$, $\Omega_C=-0.46$, $\Omega_D=6.5$.

IV. CONCLUDING REMARKS

In all simulations a cellular pattern has been found at the onset of convection in the bulk. At $\sigma=6.4(\Gamma=5,3)$, a regular square pattern is often seen in a range of small ε preceding a KL-like state with a switching angle of about 50°. The square pattern exhibits oscillations in the amplitudes of its two roll components and rotates with a small prograde velocity. Our results suggest that $\Omega_{sq}(\varepsilon,\Gamma)\to 0$ for $\Gamma\to\infty$ and show that $\Omega_{sq}(\varepsilon,\Gamma)\to 0$ for $\varepsilon\to 0$. In the case $\sigma=0.7$ with $\Gamma=3$ and insulating boundary conditions a hexagonal pattern is found which is more irregular and is disrupted by the spiral arms connected to the sidewall convection. Moreover, because of the strong interaction between wall and bulk modes the latter rotates in the retrograde direction.

The present results show that, neither deviations from the Boussinesq approximation nor the presence of the centrifugal force, which are present in the experiments, but neglected in the theory, need not be invoked to explain the occurrence of the square patterns instead of the expected Küppers-Lortz state. Moreover, as already mentioned in Ref. [10] the numerical results confirm that impurities or poorly conducting boundaries in experiments cannot serve as an explanation either. Finally, the present results show that the nature of the sidewall boundary conditions (insulating or conducting) does not influence significantly the cellular characteristics of the convection patterns in the bulk.

For an understanding of the competition between square pattern convection and convection rolls it is important to start with the fact that both patterns are unstable in an infinitely extended layer. Rolls are unstable because of the Küppers-Lortz mechanism witch tends to replace them with new rolls oriented with angle of 60° in the prograde direction relative to the given rolls. With increasing Ω this angle tends to decrease and assumes a value of only 50° as usually found in our simulations. Square pattern convection is unstable owing to the property that one of the participating rolls tends to grow at the expense of the other one. This process is noticeable in the form of small oscillations of the rolls components even in the case when a perfect square pattern seems to have been realized. The interaction with the sidewall mode appears to stabilize the square pattern mainly because rolls are always unstable where they are oriented tangentially to the sidewall. Each of the two types of rolls thus receives a boost from the part of the wall to which they are nearly orthogonal. At this point the question may arise as to why are hexagons not found instead of squares. The answer is that in contrast to the square pattern hexagons are also subject to the Küppers-Lortz instability in that in a cyclic fashion one of the three roll components is always decaying (see Refs. [4,29]). Only in the rather confined simulation of the case $\Gamma=3,\sigma=0.7$, with insulating sidewalls and with dominating sidewall convection, could the three fold coordination typical for hexagonal cells be observed.

The slow rotation in the prograde direction of the square pattern is apparently caused by the interaction with the sidewall mode. While the latter travels in the retrograde direction, the reconnections that happen persistently between sidewall and interior eddies appear to impart the slow prograde rotation on the bulk pattern. In the case of larger aspect ratio $\Gamma=5$ the fact that two subsequent Küppers-Lortz processes tend to reinforce the second roll component of the square pattern may also play a role. Because twice the preferred angle of about 50° is a bit larger than 90° the Küppers-Lortz instability thus tends to reinforce the perpendicular rolls and at the same time imparts a slow rotation in the prograde direction.

It is obvious from the preceding discussion that more detailed theoretical studies of the interaction between sidewall convection and bulk pattern convection are desirable. It is hoped that the numerical simulation presented in the paper together with the experimental observations published in the literature will stimulate such studies.

ACKNOWLEDGMENT

Thanks to the scientific committee of Centre National de la Recherche Scientifique (CNRS) Computing Center (IDRIS) for supporting this work (Research Program 0242). This research was partially supported by MEC (Projects no. BFM2001–0297 and FIS2004–06596–C02–02).

[1] G. Küppers and D. Lortz, J. Fluid Mech. **35**, 609 (1969).
[2] K. M. S. Bajaj, G. Ahlers, and W. Pesch, Phys. Rev. E **65**, 056309 (2002).
[3] K. E. Heikes and F. H. Busse, Ann. N.Y. Acad. Sci. **357**, 28 (1980).
[4] F. H. Busse and K. E. Heikes, Science **208**, 173 (1980).
[5] Y. Hu, W. Pesch, G. Ahlers, and R. E. Ecke, Phys. Rev. E **58**, 5821 (1998).

[6] Y. Hu, R. E. Ecke, and G. Ahlers, Phys. Rev. Lett. **74**, 5040 (1995).
[7] F. Zhong, R. Ecke, and V. Steinberg, Phys. Rev. Lett. **67**, 2473 (1991).
[8] E. Bodenschatz, D. S. Cannell, J. R. de Bruyn, R. Ecke, Y.-C. Hu, K. Lerman, and G. Ahlers, Physica D **61**, 77 (1992).
[9] E. Serre, E. Crespo del Arco, and F. H. Busse, in *Nonlinear Dynamics in Fluids* edited by F. Marqués and A. Meseguer (CIMNE, Barcelona, 2003), Chap. 3, pp. 138–140.
[10] M. Fantz, R. Friedrich, M. Bestehorn, and H. Haken, Physica D **61**, 147 (1992).
[11] Y. Tu and M. C. Cross, Phys. Rev. Lett. **69**, 2515 (1992).
[12] J. Millan-Rodriguez, M. Bestehorn, C. Pérez-García, R. Friedrich, and M. Neufeld, Phys. Rev. Lett. **74**, 530 (1995).
[13] L. Ning and R. E. Ecke, Phys. Rev. E **47**, 3326 (1993).
[14] Y. Liu and R. E. Ecke, Phys. Rev. Lett. **78**, 4391 (1997).
[15] Y. Liu and R. E. Ecke, Phys. Rev. E **59**, 4091 (1999).
[16] R. E. Ecke and Y. Liu, Int. J. Eng. Sci. **36**, 1471 (1998).
[17] H. F. Goldstein, E. Knobloch, I. Mercader, and M. Net, J. Fluid Mech. **248**, 583 (1993).
[18] J. Hermann and F. H. Busse, J. Fluid Mech. **255**, 183 (1993).
[19] E. Y. Kuo and M. C. Cross, Phys. Rev. E **47**, R2245 (1993).
[20] J. Scheel, M. Paul, M. Cross, and P. Fischer, Phys. Rev. E **68**, 066216 (2003).
[21] R. M. Clever and F. H. Busse, J. Fluid Mech. **94**, 609 (1979).
[22] K. M. S. Bajaj, J. Liu, B. Naberhuis, and G. Ahlers, Phys. Rev. Lett. **81**, 806 (1998).
[23] E. Bodenschatz, W. Pesch, and G. Ahlers, Annu. Rev. Fluid Mech. **32**, 709 (2000).
[24] R. Peyret, *Spectral Methods for Incompressible Viscous Flow*, Applied Mathematical Sciences Vol.148 (Springer, New York, 2002).
[25] I. Raspo, S. Hugues, E. Serre, A. Randriamampiana, and P. Bontoux, Comput. Fluids **31**, 745 (2002).
[26] E. Serre and J. P. Pulicani, Comput. Fluids **30**, 491 (2001).
[27] M. Net and I. Mercader (private communication).
[28] S. Chandrasekhar, *Hydrodynamic and Hydromagnetic Stability* (Dover, New York, 1961).
[29] F. H. Busse, in *Turbulence and Chaotic Phenomena in Fluids*, edited by T. Tatsumi (Elsevier, 1984), pp. 197–202.